The Journal of Neuroscience, April 15, 2001, *21*(8):2878–2888

Propagation of Neocortical Inputs in the Perirhinal Cortex

Marzia Martina, Sébastien Royer, and Denis Paré

Laboratoire de Neurophysiologie, Département de Physiologie, Faculté de Médecine, Université Laval, Québec City, (QUE), Canada, G1K 7P4

The perirhinal area is a rostrocaudally oriented strip of cortex in which lesions produce memory and perceptual impairments. It receives topographically organized transverse projections from associative neocortical areas and is endowed with intrinsic longitudinal connections that could distribute neocortical inputs in the rostrocaudal axis. In search of distinguishing network properties that might support perirhinal involvement in memory, we have performed whole-cell recordings in horizontal perirhinal slices with preserved transverse neocortical links and intrinsic longitudinal connections. Neocortical stimulation sites in rostrocaudal register with regular spiking perirhinal neurons elicited a sequence of excitatory and inhibitory synaptic potentials. In contrast, apparently pure excitatory responses were observed when the stimulating and recording sites were separated by ≥1 mm in the rostrocaudal axis. This suggested that adjacent and distant neocortical stimuli influence regular spiking perirhinal neurons by pathways that respectively form and do not form synapses with inhibitory interneurons. In keeping with this, presumed interneurons did not respond to distant neocortical stimuli. These results suggest that neocortical inputs recruit perirhinal inhibitory interneurons located at the same transverse level, limiting the depolarization of principal perirhinal cells. In contrast, distant neocortical inputs only evoke excitation because longitudinal perirhinal pathways do not engage inhibitory interneurons. This leads us to suggest that the perirhinal network is biased to favor Hebbian-like associative interactions between coincident and spatially distributed inputs.

Key words: perirhinal; neocortex; inhibition; horizontal connections; learning; memory

In the fundus and lateral bank of the rhinal fissure are cortical areas collectively known as the perirhinal cortex. These areas are believed to play a critical role in high-order perceptual and mnemonic functions, because perirhinal lesions interfere with recognition and associative memory in various sensory modalities (Zola-Morgan et al., 1989, 1993; Bunsey and Eichenbaum, 1993; Meunier et al., 1993, 1996; Suzuki et al., 1993; Eacott et al., 1994; Mumby and Pinel, 1994; Higuchi and Miyashita, 1996; Herzog and Otto, 1997; Buckley and Gaffan, 1998). Moreover, perirhinal neurons exhibit various types of memory-related activity such as familiarity or novelty effects and stimulus-selective delay firing in delayed matching-to-sample tasks (for review, see Suzuki, 1996).

In keeping with this, the perirhinal cortex occupies a strategic position among temporal lobe structures involved in declarative memory (for review, see Zola-Morgan and Squire, 1993). Indeed, in all species studied so far, it was found that the perirhinal cortex relays most neocortical sensory inputs to the entorhinohippocampal system and represents the main return path for hippocampo-entorhinal efferents to the neocortex (Jones and Powell, 1970; Van Hoesen and Pandya, 1975; Deacon et al., 1983; Room and Groenewegen, 1986; Witter and Groenewegen, 1986; Witter et al., 1986; Insausti et al., 1987; Suzuki and Amaral, 1994a,b; Burwell and Amaral, 1998a,b; Shi and Cassell, 1999).

Most neocortical afferents to the perirhinal cortex originate from association cortical areas, particularly from those bordering the perirhinal cortex laterally (Deacon et al., 1983; Room and Groenewegen, 1986). Moreover, neocortical projections are organized topographically, with rostral cortical areas concentrating on rostral perirhinal levels and posterior ones focusing on more caudal parts of the perirhinal cortex (Deacon et al., 1983; Room and Groenewegen, 1986). Superimposed on these topographically organized transverse neocortical projections is an intrinsic system of longitudinal connections that spans the entire rostrocaudal extent of the perirhinal cortex (Witter et al., 1986).

In light of the deficits produced by perirhinal lesions, an attractive possibility is that intrinsic perirhinal axons relate coincident neocortical activation patterns targeting different rostrocaudal levels of the perirhinal cortex. Indeed, the associative potential of such network interactions might be critical for the involvement of the perirhinal cortex and related areas in memory (Eichenbaum, 1993, 1997). However, the physiological organization of the perirhinal network has received little attention so far.

Thus, we have developed a method for obtaining horizontal slices of the perirhinal cortex that preserve its transverse links with the neocortex and its intrinsic connections. Using whole-cell recordings as well as chemical and electrical stimulation, we have analyzed the propagation of neocortical influences in the perirhinal cortex. Our results suggest that the effects of neocortical inputs on perirhinal neurons depend on whether neocortical afferents and recipient perirhinal cells are in transverse register or not, because of differential interactions with inhibitory interneurons.

MATERIALS AND METHODS

Preparation of perirhinal slices. Coronal or horizontal slices of the perirhinal cortex were obtained from Hartley guinea pigs (250–300 gm). This species was chosen because the position and orientation of the rhinal sulcus makes it possible to obtain horizontal perirhinal sections. Indeed,

Received Nov. 2, 2000; revised Jan. 22, 2001; accepted Jan. 26, 2001.

This work was supported by the Natural Sciences and Engineering Research Council and the Medical Research Council of Canada. We thank D. R. Collins and E. J. Lang for comments on an earlier version of this manuscript.

Correspondence should be addressed to Denis Paré, Département de Physiologie, Faculté de Médecine, Université Laval, Québec City, (QUE), Canada, G1K 7P4. E-mail: denis.pare@phs.ulaval.ca.

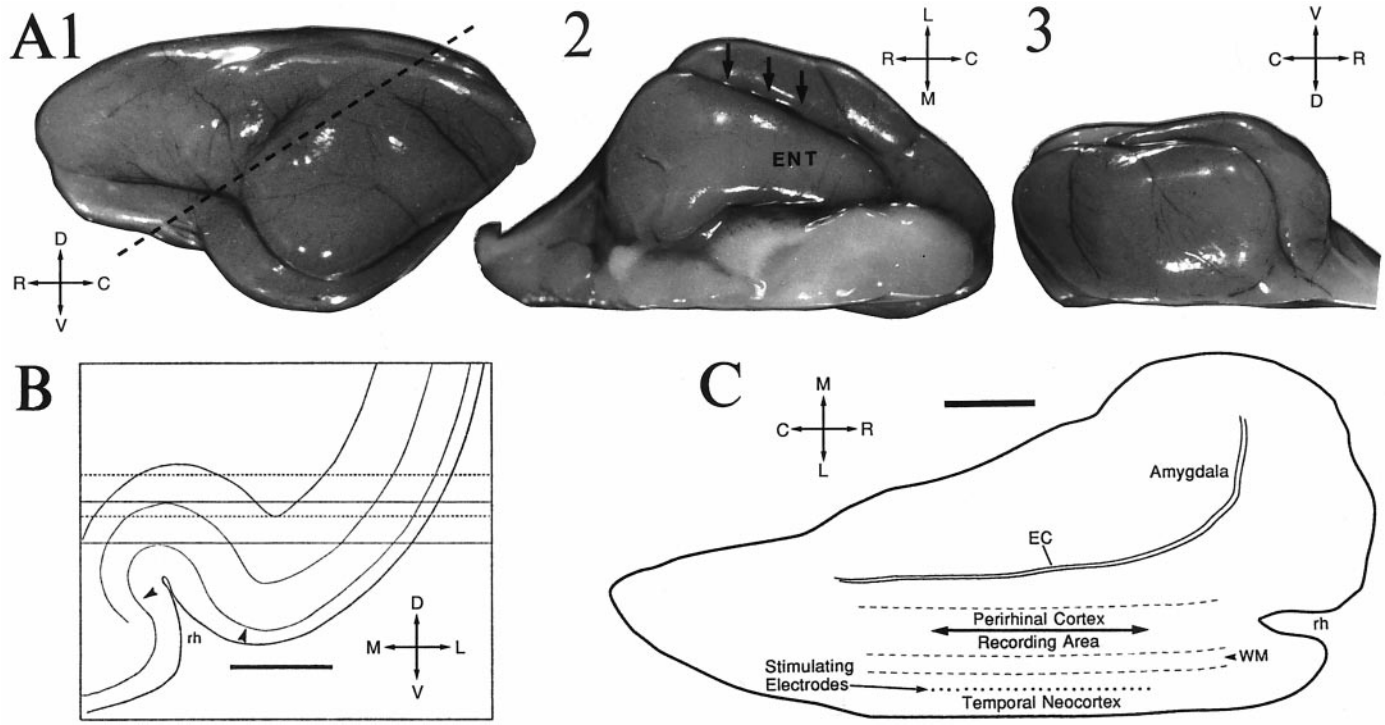

Figure 1. Preparation of horizontal perirhinal slices. The orientation of each panel is indicated by *arrows* (*C*, caudal; *D*, dorsal; *L*, lateral; *M*, medial; *R*, rostral; *V*, ventral). *A1*, In a hemisphere resting on its medial aspect, a rostrocaudal cut parallel to the rhinal sulcus was performed (*dashed line*). *A2*, The block was glued to the stage of the vibrating microtome with its ventral aspect facing upward. *Arrows* indicate how the blade approached the block laterally. *A3*, Lateral view of the block. *B*, Scheme of a coronal section through the perirhinal cortex. *Arrowheads* to the *left* and *right* of the rhinal sulcus (*rh*) indicate the medial and lateral limits of the perirhinal cortex (areas 35 and 36). Laterally, the perirhinal cortex is bordered by associative neocortical areas. The *continuous* and *dashed horizontal lines* depict the cortical tissue included in the horizontal sections obtained as described in *A*. *C*, Horizontal perirhinal slice as it appeared in the recording chamber. Scale bars: *B*, *C*, 1 mm. *EC*, External capsule; *WM*, white matter.

the rhinal sulcus of the guinea pig exhibits no curvature over a large portion of its rostrocaudal extent.

In agreement with the guidelines of the Canadian council on animal care, the animals were deeply anesthetized with sodium pentobarbital (40 mg/kg, i.p.) plus ketamine (100 mg/kg, i.p.) and then decapitated. The brain was removed rapidly and placed in a cold (4°C) oxygenated solution containing (in mM): 126 NaCl, 2.5 KCl, 1.25 NaH_2PO_4, 1 $MgCl_2$, 2 $CaCl_2$, 26 $NaHCO_3$, and 10 glucose. A block containing the perirhinal cortex was prepared, and sections (400 μm) were obtained using a vibrating microtome. The slices were stored for 1 hr in an oxygenated chamber at room temperature. One slice was then transferred to a recording chamber (submerged type) and perfused with an oxygenated physiological solution at a rate of 2 ml/min. The temperature of the chamber was gradually increased to 32°C before the recordings began.

Horizontal sections of the perirhinal cortex were obtained in the following manner. After the two hemispheres were separated, a rostrocaudal cut parallel to the rhinal sulcus was performed as shown in Figure 1*A1* (*dashed line*). Then, the dorsal aspect of the brain was glued to the stage of the vibrating microtome with its ventral aspect upward (Fig. 1*A2*), as shown from profile in Figure 1*A3*. The vibrating blade thus approached the brain laterally (Fig. 1*A2*, *arrows*), resulting in 400 μm horizontal slices including the neocortex laterally (Fig. 1*B*,*C*) and the amygdala rostrally (Fig. 1*C*). Each hemisphere yielded only one horizontal section of the perirhinal cortex.

Data recording and analysis. Under visual guidance using differential interference contrast and infrared video microscopy (IR-DIC), current-clamp recordings were obtained with borosilicate pipettes filled with a solution containing (in mM): 130 K-gluconate, 10 HEPES, 10 KCl, 2 $MgCl_2$, 2 ATP-Mg, and 0.2 GTP-Tris. In some experiments, Neurobiotin (0.5%) was added to the intracellular solution for morphological identification of the cells (see below). pH was adjusted to 7.2 with KOH, and osmolarity was adjusted to 280–290 mOsm. The liquid junction potential was measured (10 mV), and the membrane potential (V_m) was corrected accordingly after the experiments. All V_m values reported in the text were corrected for the junction potential. The pipettes had resistances of 4–7 MΩ when filled with the above solution. Recordings with series resistance >15 MΩ were discarded.

The electroresponsive properties of perirhinal neurons were investigated by applying 0.2–5 sec current pulses from rest and one or more prepulse potentials, as determined by steady current injection. The amplitude of current pulses was varied in fixed increments of 10 pA.

Neocortical stimulation. An array of 28 tungsten electrodes (tip diameter, 25 μm; intertip spacing, 160 μm) was positioned in the deep layers of the adjacent temporal neocortical field, as shown in Figure 1*C* (*dots*). Bipolar electrical stimuli consisted of 100 μsec current pulses (0.1–1.2 mA; 0.1 Hz) passed through neighboring electrodes. These synaptic responses were elicited from a V_m of approximately −65 mV as determined by intracellular current injection. When we studied synaptic responses elicited by electrical stimulation of the neocortex, the stimulation intensity at the neocortical site closest to the recorded cell was increased gradually in steps of 50 μA until a response was evoked. Then, all the stimulation sites were scanned sequentially at the threshold intensity (usually between 0.15 and 0.3 mA) and at two or more higher stimulation intensities. Four stimuli were applied at each site and stimulus strengths and averaged independently. A site was considered responsive only if, at a particular stimulus intensity, at least three of the four stimuli elicited a response at a constant latency. Synaptic events with amplitudes ≤0.5 mV were ignored.

Local injections of glutamate were performed in the neocortex by applying air pressure pulses (6–50 msec) to micropipettes (inner diameter of the tip: ~0.8 μm) containing 0.5 mM glutamate (dissolved in the extracellular solution). The slices were oriented so that the ejected glutamate would diffuse away from the recorded cell, carried by the flow of the extracellular solution toward the chamber outlet. To determine whether glutamate leaked from the ejection pipette, we compared the amount of spontaneous synaptic activity (quantified by computing the SD of the intracellular signal) displayed by neurons recorded in the presence versus absence of glutamate-filled pipettes. No differences were observed.

Analyses were performed off-line with the software IGOR (Wave-

Table 1. Physiological properties of perirhinal neurons

Cell type	Incidence (%)	V_m (mV)	R_{in} (MΩ)	τ (msec)	Spike amplitude (mV)	Spike duration at half-amplitude (msec)
Regular spiking ($n = 159$)	81	−80 ± 0.7	193 ± 9.17	30.6 ± 1.42	87.5 ± 1.11	1.1 ± 0.02
Bursting ($n = 16$)	8	−79 ± 1.3	230 ± 54.0	28.5 ± 2.15	92.4 ± 1.5	1.0 ± 0.07
Fast spiking ($n = 16$)	8	−70 ± 2.1	264 ± 22.2	15.8 ± 2.78	84.3 ± 2.2	0.4 ± 0.05

metrics) and homemade software running on Macintosh microcomputers. The input resistance (R_{in}) of the cells was estimated in the linear portion of current–voltage plots. The membrane time constant was derived from single exponential fits to voltage responses in the linear portion of current–voltage relations. Spike afterhyperpolarizations (AHPs) were measured using the lowest current amplitudes eliciting at least two spikes and by considering the spike thresholds as reference points. All values are expressed as means ± SE.

Morphological identification of recorded cells. When recorded cells were dialyzed with Neurobiotin, the slices were removed from the chamber and fixed for 1–3 d in 0.1 M PBS, pH 7.4, containing 2% paraformaldehyde and 1% glutaraldehyde. Slices were then embedded in gelatin (10%) and sectioned on a vibrating microtome at a thickness of 60–100 μm. Neurobiotin-filled cells were visualized by incubating the sections in the avidin–biotin–horseradish peroxidase (HRP) solution (ABC Elite Kit, Vector Laboratories, Burlingame, CA) and processed to reveal the HRP staining.

RESULTS

Database

A total of 241 perirhinal neurons generating overshooting action potentials and having a corrected V_m of at least −60 mV were recorded in this study. Because neurons with different electroresponsive properties exhibited dissimilar synaptic response profiles, we will first describe the physiological properties of perirhinal neurons and then analyze their responses to neocortical inputs.

Electroresponsive and morphological properties of perirhinal neurons

In these experiments, pipettes were aimed to the somatic profiles closest to the pipette tip, regardless of their diameter (50 and 146 cells in coronal and horizontal slices, respectively) (Table 1). In agreement with previous findings (Beggs and Kairiss, 1994; Faulkner and Brown, 1999), perirhinal neurons displayed various electroresponsive properties, similar to that observed in neocortical areas (Connors et al., 1982; Stafstrom et al., 1984; McCormick et al., 1985; Nuñez et al., 1993; Schwindt et al., 1997), but with significant differences. We observed three main types of cells, hereafter termed regular spiking (RS), burst firing (BF), and fast-spiking (FS) neurons (Table 1). These three cell types were encountered in all cortical layers with the exception of layer I and accounted for 81, 8, and 8% of our sample, respectively.

RS neurons

Like their neocortical counterpart, RS neurons generated spike trains that exhibited various degrees of frequency adaptation when depolarized. This is illustrated in Figure 2*A*, where the first current pulse eliciting at least one spike is shown, along with the response to a larger depolarizing current injection (*top trace*). From cell to cell, the spike AHPs generated by RS neurons varied greatly, ranging from long biphasic AHPs to short monophasic ones (range, 45–199 msec; average, 129.7 ± 8.19 msec).

BF neurons

To be classified as such, BF cells had to meet one of the two following criteria: their first suprathreshold response consisted of (1) an initial spike burst or doublet (first interspike interval 6.9 ± 0.51 msec) or (2) a single spike followed by an afterdepolarization (ADP) (Fig. 2*B*, *arrow*) that gave rise to two or more spikes when larger current injections were performed (Fig. 2*B*, *top trace*). In four of five tested cells, depolarization of the prepulse V_m above −65 mV abolished the spike bursts and the ADPs. In terms of repetitive firing properties, BF cells differed from RS cells only in their initial response to depolarizing current injections; after the initial burst, they displayed a continuum of spike frequency adaptation similar to that exhibited by RS cells. The resting potential, spike duration, R_{in}, and time constant of BF cells did not differ significantly from those of RS neurons (Student's unpaired *t* tests, $p > 0.05$) (Table 1).

FS neurons

These cells could sustain high firing rates (up to 100 Hz) for prolonged periods of time (longest tested interval: 5 sec) with little or no spike frequency adaptation (Fig. 2*C*). Compared with RS cells, these neurons had a more positive resting potential, a higher R_{in}, and a shorter membrane time constant (Table 1). In addition, their AHPs were shorter in duration (15.7 ± 2.43 msec; $n = 8$), and they generated briefer action potentials (hence the designation "fast-spiking" neurons). All these differences were statistically significant (Student's unpaired *t* tests, $p < 0.05$).

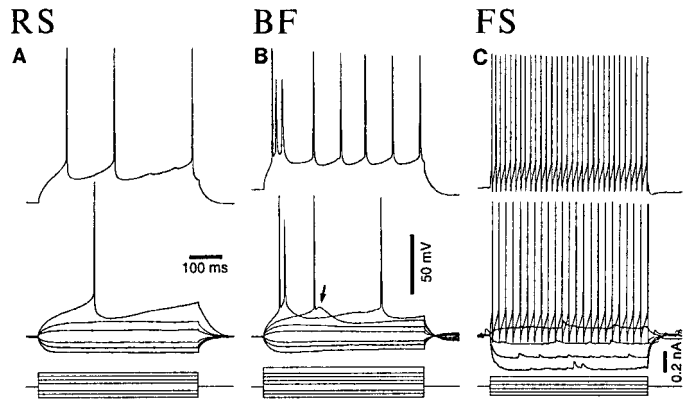

Figure 2. Electroresponsive properties of perirhinal neuron. *A–C*, Three different perirhinal cells. *A*, *RS; B*, *BF*; *C*, *FS* neuron. Voltage responses to graded series of current pulses were applied from rest. For each cell, the first suprathreshold current pulse is shown along with the response to one or more larger depolarizing current injection (*top trace*). In this and the following Figures, current injections were increased in fixed steps of 10 pA but only selected current injections are shown. Rest was −82, −74, and −72 mV in *A–C*, respectively.

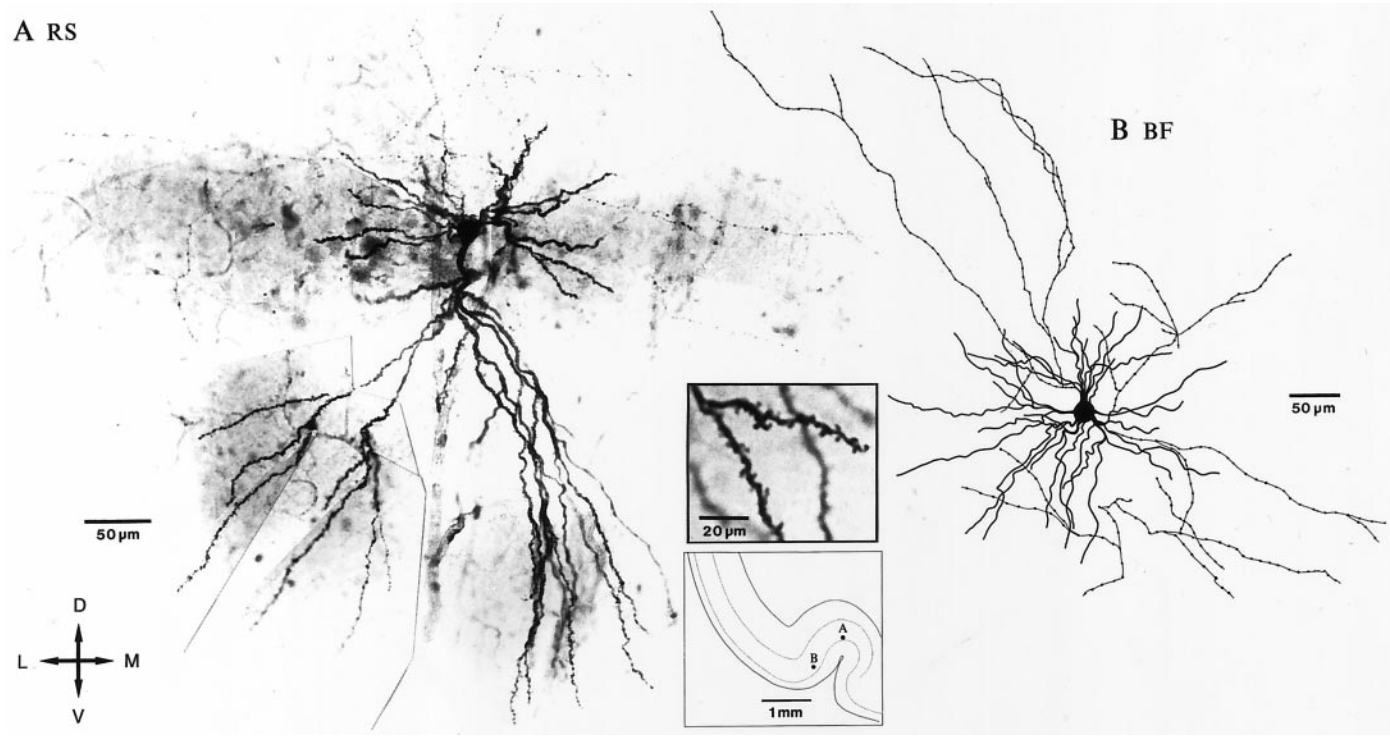

Figure 3. Morphological properties of RS (*A*) and BF (*B*) neurons. The neurons were recorded at the position indicated in the scheme at the *bottom right* of *A*. The orientation of the Figure is indicated by the *cross* on the *left*. The *inset* in *A* shows a spiny dendritic segment. *D*, Dorsal; *L*, lateral; *M*, medial; *V*, ventral.

Morphological features

The morphological features of RS ($n = 13$) (Fig. 3*A*) and BF ($n = 3$) (Fig. 3*B*) neurons overlapped extensively. Both types ranged in morphology from pyramidal (Fig. 3*A*) to stellate (Fig. 3*B*); however, all had spiny dendrites (Fig. 3*A*, *inset*). In contrast, all FS neurons ($n = 5$) had aspiny dendrites (Fig. 4*B*). Their dendritic branches radiated in stellate to bitufted (Fig. 4*A*) configurations from ovoid cell bodies.

Differences in soma size between FS, RS, and BF cells did not reach significance when measurements were made on Neurobiotin-filled neurons (longest axis: RS, 23.5 ± 1.22 μm; BF, 24.3 ± 1.87 μm; FS, 22.2 ± 1.67 μm; Student's unpaired *t* test, $p < 0.05$; $n = 13$, 3, and 5 cells, respectively). In contrast, when we used values obtained with IR-DIC just before the recordings, the somata of FS neurons (10.1 ± 0.63 μm; $n = 8$) were significantly smaller than those of RS (23.9 ± 1.28 μm; $n = 20$) and BF cells (24.1 ± 1.77 μm; $n = 8$; Student's unpaired *t* tests, $p < 0.05$). The discrepancy probably resulted from the distortion caused when the pipettes were retracted from the cells.

Thus, in the experiments described below, pipettes were aimed toward somatic profiles with small diameters, to increase the likelihood of recording FS cells. Forty-five perirhinal neurons were recorded in this manner, all in horizontal slices. Because we lacked morphological criteria to increase the likelihood of recording BF cells and because their synaptic response profile to neocortical stimuli seemed identical to that of RS neurons, the following section will focus on the synaptic responsiveness of RS and FS neurons.

Synaptic response profile of RS perirhinal neurons to neocortical stimuli

The effects of neocortical stimuli applied at different rostrocaudal levels (Fig. 1*C*, *dots*) were examined in 99 RS neurons. As a rule, RS cells were responsive to a majority of stimulation sites, the spatial extent of effective sites remaining constant once the stimulus strength had reached ~1.2 times the response threshold of the stimulation site closest to the recorded cell. Further increases in stimulation intensity (up to six times threshold) changed response amplitudes but not their nature.

The synaptic response profiles of three RS cells is shown in Figure 5. Note that regardless of the cells' position (*triangles* at the bottom of the histograms), the character of the responses changed with the distance between the recorded cell and the stimulation site. When the distance was short, responses were composed of excitatory and inhibitory components (Fig. 5*A2*, sites *1*, *5*, and *7*; Fig. 5*B2*, sites *9*, *13*, and *19*; Fig. 5*C2*, sites *12*, *17*, and *21*). In contrast, distant sites elicited apparently pure excitatory responses (Fig. 5*A2*, sites *15* and *18*; Fig. 5*B2*, sites *2* and *25*; Fig. 5*C2*, sites *5* and *25*). On average, the transition from mixed (excitatory–inhibitory) to seemingly pure excitatory responses occurred at a distance of 6.1 ± 0.31 sites from the cells (or 960 ± 49.6 μm). Overall, this phenomenon was observed in 88% of tested neurons.

A simple explanation for the above results would be that neocortical stimuli applied at the same rostrocaudal level directly activate (by current spread) GABAergic neurons projecting to RS cells. At odds with this explanation, however, is that excitatory and inhibitory responses to neocortical stimuli were abolished by addition of the non-NMDA receptor antagonist 6-cyano-7-nitroquinoxaline-2,3-dione (CNQX; 20 μM; $n = 5$) to the perfusate, in agreement with previous findings (Bilkey, 1996; Ziakopoulos et al., 1999). This observation implies that the IPSPs were generated by the glutamatergic activation of perirhinal inhibitory interneurons by neocortical and/or perirhinal axons.

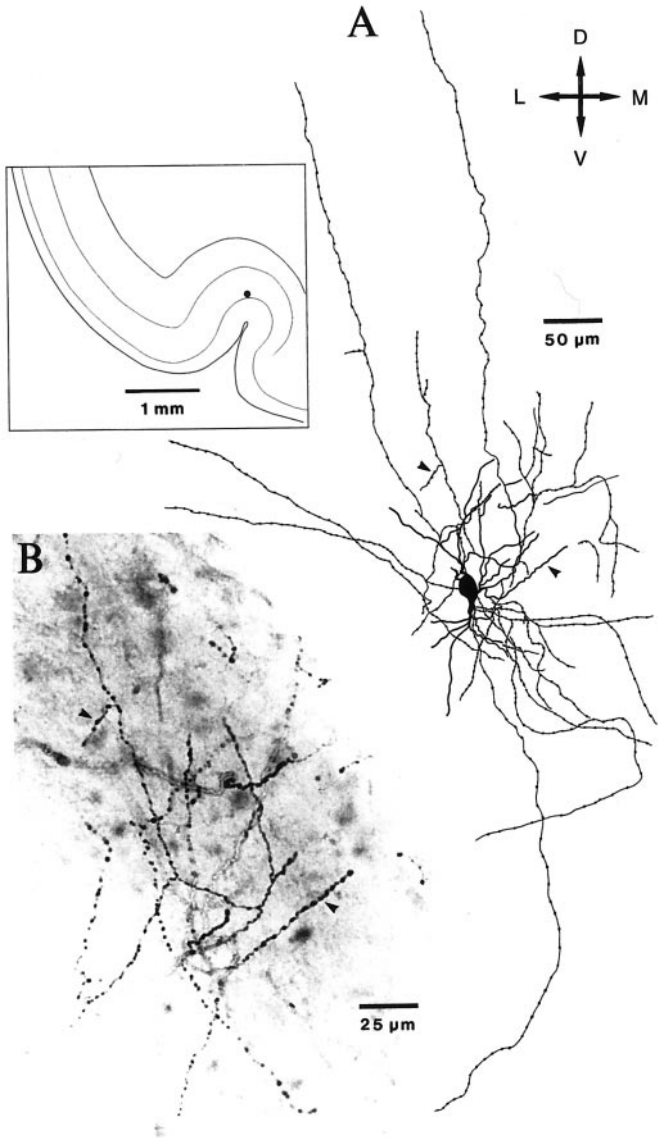

Figure 4. Morphological properties of a FS neuron. The neuron recorded is at the position indicated in the scheme on the *left*. The *arrowheads* in *A* mark segments shown at a higher magnification in *B*. The orientation of the Figure is indicated by the *cross* on the *top right*. *D*, Dorsal; *L*, lateral; *M*, medial; *V*, ventral.

Examination of inhibitory responses elicited by adjacent neocortical stimuli at different V_m values (Fig. 6) revealed that they were composed of two components: an early one (Fig. 6*A*, ▲), reversing at -69.5 ± 3.12 mV ($n = 9$), and a late one (Fig. 6*A*, ●), the amplitude of which became nil at a more negative V_m (-92.3 ± 4.11 mV; $n = 9$). When electrical stimuli were delivered at proximity of recorded cells (in the perirhinal cortex), but in the presence of CNQX (20 μM) and AP-5 (100 μM), the GABA-A receptor antagonist bicuculline (10 μM) markedly reduced the early phase of the IPSP (reduction of $88 \pm 5.2\%$; $n = 5$), whereas the GABA-B antagonist saclofen (100 μM) reduced the late phase by $46 \pm 4.9\%$ ($n = 4$). These results are consistent with the biphasic GABAergic responses observed in other cortical fields and species that are mediated by a Cl^- (GABA-A) and a K^+ (GABA-B) conductance (Dutar and Nicoll, 1988; McCormick, 1989; Scanziani et al., 1991).

In contrast, the extrapolated reversal potential of synaptic responses evoked by distant stimulation sites was much more positive (Fig. 6*B*). It averaged -18.5 ± 8.47 mV ($n = 7$) when measured at a latency corresponding to the peak of the early IPSP elicited by adjacent stimulation sites.

Origin of the differences between responses to adjacent and distant stimulation sites

The differences between the effect of stimuli applied at distant versus adjacent neocortical sites lend themselves to several interpretations. A first possibility is that the afferent volley evoked by distant sites is insufficient to drive inhibitory interneurons contacting the recorded cells. A second possibility is that adjacent, but not distant, stimulation sites backfire some perirhinal neurons having axon collaterals that excite neighboring inhibitory cells (i.e., feedback inhibition). A third possibility is that the pathways conveying the volley elicited by adjacent and distant cortical stimuli, respectively, form and do not form synaptic contacts with inhibitory neurons.

To test the first possibility, we examined the synaptic responses elicited by adjacent and distant neocortical stimuli in a larger range of stimulation intensities (Fig. 7) than used in previous figures. In all but one of the tested cells ($n = 8$), adjacent neocortical stimuli elicited an excitatory–inhibitory response at all intensities from the lowest stimulus amplitude evoking a response (Fig. 7*A*, *0.3 mA*) to the strongest stimuli that our equipment could deliver (*1.2 mA*). In the eighth neuron, an apparently pure inhibitory response was first seen at the lowest stimulation intensity. EPSPs appeared when the stimulation intensity was increased.

The character of the responses elicited by distant stimulation sites (Fig. 7*B*) remained unchanged at all subthreshold intensities and in all tested cells ($n = 8$). In Figure 7*B*, note that we did not illustrate intensities higher than 0.9 mA because they elicited action potentials. Because reducing the intensity of adjacent stimuli or increasing that of distant ones did not modify the character of evoked responses, it appears unlikely that the differing intensity of the afferent volley is responsible for the contrasting responses evoked by adjacent and distant cortical stimuli.

Thus, we turned our attention to the possibility that the differing responses evoked by adjacent and distant stimulation sites resulted from the fact that adjacent sites had a higher probability of backfiring perirhinal cells with excitatory collaterals to local interneurons. We reasoned that this explanation would appear very unlikely if the effects of adjacent electrical stimuli could be reproduced by chemical stimuli that excited neocortical cells without affecting perirhinal axons. Accordingly, we examined the effect of local pressure application of glutamate through a patch pipette in neocortical sites adjacent to ($n = 5$) or distant from (>2 mm; $n = 4$) the recorded perirhinal cells. In these experiments, the orientation of the slice in the recording chamber was adjusted so that the direction of the ringer flow would facilitate glutamate diffusion away from the recorded cells to prevent direct glutamate effects on perirhinal neurons.

These chemical stimuli elicited a response dominated by inhibition when applied at the same rostrocaudal level as the recorded cell (in five of five tested cells) (Fig. 8*A*) and depolarizing responses when applied at distant sites (in three of four tested cells, the fourth cell was unresponsive; data not shown). Both observations were obtained in two or more slices. At −65 mV, peak inhibitory and excitatory responses evoked by adjacent and

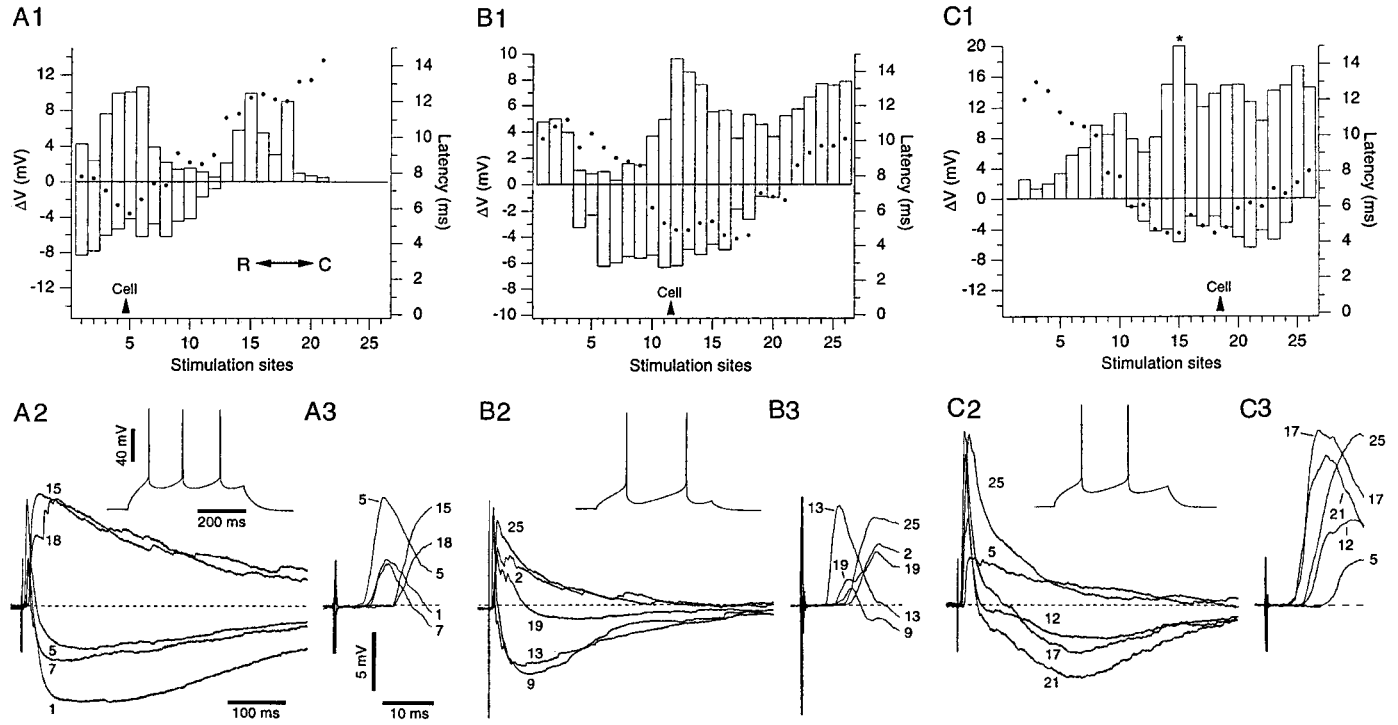

Figure 5. Relationship between the response profile of RS cells and their rostrocaudal position. Shown are synaptic responses of three different neurons (*A–C*) to electrical stimuli (100 μsec; 1.4 times the threshold intensity) applied in the neocortex. Stimulating sites were 160 μm apart. *A1*, *B1*, *C1*, Graphs plotting the peak amplitude (*bars*, *left axis*) of evoked synaptic potentials as a function of the stimulation site (average of four responses). The onset latency of the EPSPs is also indicated (*dots*, *right axis*). The position of the recorded cells with respect to the stimulation sites is indicated by a *triangle* at the *bottom* of each graph. *A2–3*, *B2–3*, *C2–3*, Synaptic responses elicited by selected stimulation sites (*numbers*) depicted with a slow (*2*) and fast (*3*) time base (single sweeps). The *insets* in *2* illustrate the first response to depolarizing current injections eliciting more than one spike when current injections were increased in steps of 0.01 nA from rest. Calibration bars in *A* are also valid for *B* and *C*. The *asterisk* in *C* marks a suprathreshold response. In *A–C*, rest was −80, −79, and −82 mV, respectively. To depolarize the cells to −65 mV, a steady depolarizing current of 0.07, 0.06, and 0.1 nA was injected in *A–C*, respectively.

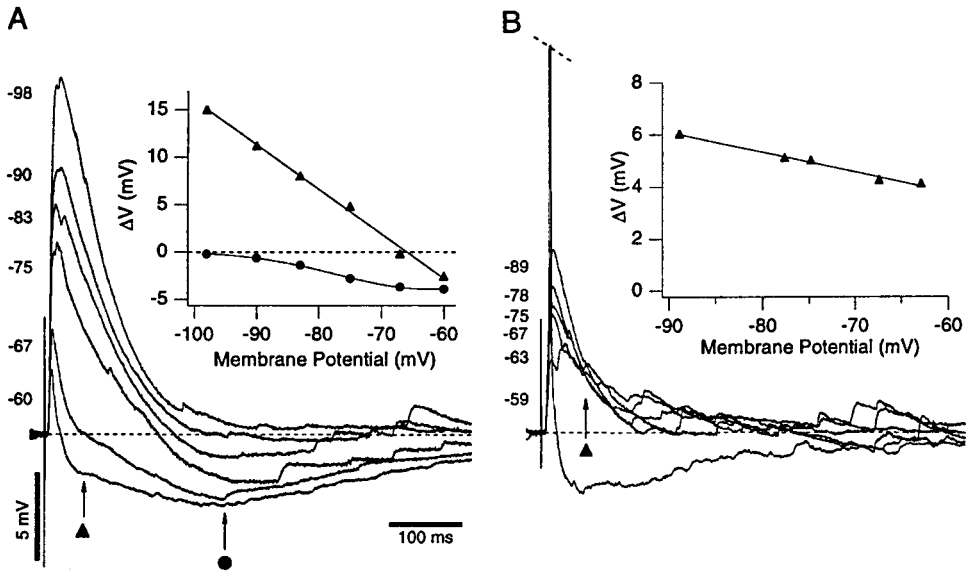

Figure 6. Effect of membrane polarization on cortically evoked responses. With respect to the recorded cell, the stimulation sites were located at the same (*A*) or at a distant rostrocaudal level (*B*). The *graphs* show how the response amplitude changed with the V_m (*numbers* on the *left* of traces), as determined by intracellular current injection. Amplitude measurements were performed at fixed intervals indicated by *symbols*. In *B*, note that the only response with a hyperpolarizing component occurred when the V_m was depolarized to −59 mV and the EPSP triggered a spike (truncated). This suprathreshold response was not considered in the *inset*. Rest was −79 mV.

distant stimuli, respectively, averaged 4.0 ± 0.38 and 7.6 ± 1.89 mV. By chance, the effect of local glutamate application in the neocortex could also be studied in one FS neuron recorded at the same rostrocaudal level as the ejection pipette. Excitatory responses were evoked (Fig. 8*B*). In this cell, no response could be elicited from distant sites.

Synaptic response profile of FS perirhinal neurons to neocortical stimuli

If the differing nature of responses elicited by adjacent and distant neocortical stimuli resulted from the fact that pathways conveying short- or long-range neocortical influences interact differentially with inhibitory interneurons, the spatial extent of stimulation sites

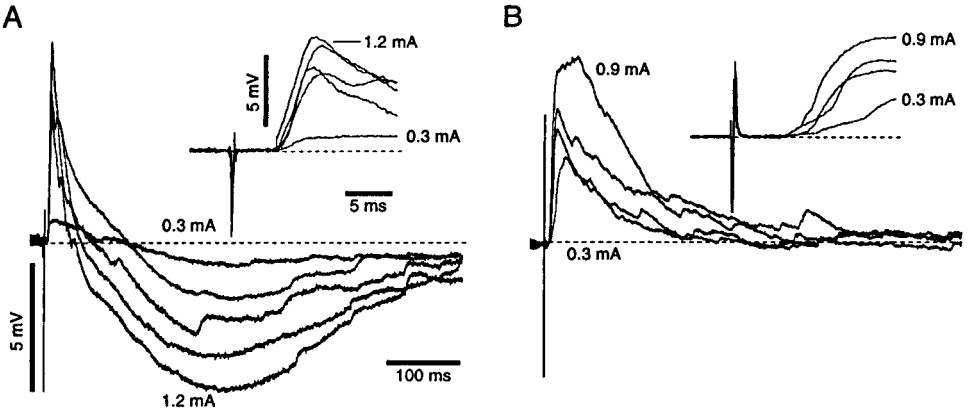

Figure 7. Effect of increasing the stimulation intensity on the responses elicited by adjacent (*A*) and distant (*B*) neocortical stimuli in RS perirhinal neurons from −65 mV. Single sweeps are shown. The threshold intensity was 0.3 mA for both stimulation sites. *Insets* show initial part of the responses with a faster time base. Superimposed sweeps show responses elicited by stimuli of 0.3, 0.4, 0.7, 0.9, and 1.2 mA in *A* and 0.3, 0.4, 0.7, 0.9 in *B*. Higher stimulation intensities evoked spikes in *B*. Rest was −78 mV.

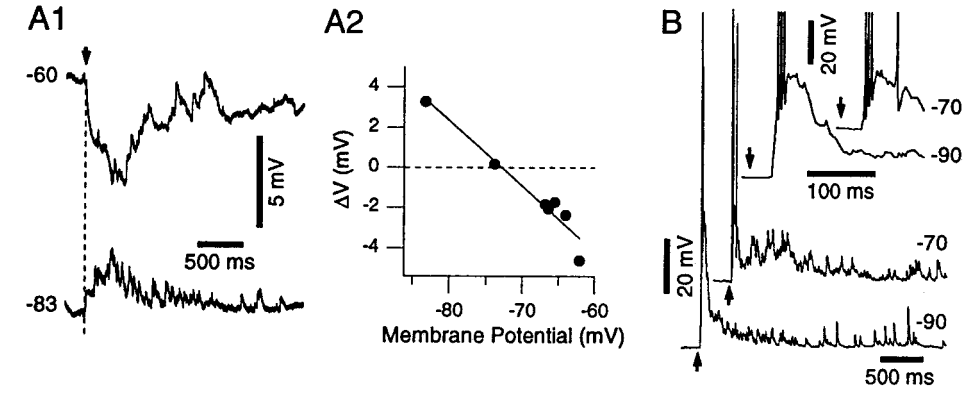

Figure 8. Local application of glutamate in the neocortex mimics the effects of electrical stimuli. Response of a RS (*A*) and a FS (*B*) neuron to local pressure injection of glutamate (30 msec pulse) in neocortical injection sites located at the same rostrocaudal level as the recorded cells is shown. In *A1* and *B*, the responses are shown at two different V_m values indicated on the *left* and *right*, respectively. *Arrows* indicate the onset of the glutamate pulse. The graph in *A2* plots the response amplitude (measured 330 msec after the stimulus onset) as a function of the V_m. The *inset* in *B* shows the responses with a faster time base (spikes are truncated). Rest was −80 and −65 mV in *A* and *B*, respectively.

exciting interneurons should be more restricted than in RS cells. To test this prediction, we examined the response profile of conventional FS cells ($n = 15$) because these neurons exhibit morphological features identical to those of GABA-immunoreactive local circuit neurons identified in Golgi studies (Ribak, 1978; Freund et al., 1983).

Figure 9 illustrates the responses of two FS cells to neocortical stimuli applied at different rostrocaudal levels. In contrast with RS neurons (Fig. 5), cortical stimuli did not evoke overt inhibition at −65 mV in FS cells (Fig. 9*A2*, *B2*). In addition, the spatial extent of stimulation sites eliciting synaptic responses seemed more restricted in FS than in RS neurons, even at the maximal stimulation intensity (1.2 mA in Fig. 9).

To address this issue quantitatively, the number of stimulation sites eliciting synaptic responses in RS and FS cells was counted. Note that this approach underestimates the number of effective sites in RS cells because many of them were responsive to all sites (Fig. 5*B*). Nevertheless, the number of sites evoking synaptic responses was significantly lower in FS than in RS neurons (19.1 ± 1.39 and 25.3 ± 0.39 sites, respectively; $n = 15$ and 25 cells; Student's unpaired t test, $p < 0.05$).

This is evident in the population histograms of Figure 10 showing the average response profile of eight RS (Fig. 10*A*) and five FS (Fig. 10*B*) cells. These cells were selected because they were recorded within 1.12 mm (or seven stimulation sites) of either extremity of the stimulating electrode array. See legend of Figure 10 for details.

Axonal path of long-range projections from the neocortex to the perirhinal cortex

Next, we performed experiments designed to identify the trajectory of pathways conveying long-range neocortical influences. Figure 11*A* illustrates the paradigm used in these experiments. RS perirhinal cells were recorded in a zone corresponding to the midpoint of our electrode array (Fig. 11*A*, ●) in slices prepared with transverse cuts at the level of stimulation site 20 (Fig. 11*A*, *black lines* labeled *B–E*). The cuts were performed under visual control with a microknife attached to a micromanipulator, and the effects of each cut were tested in at least three different slices.

After neocortical cuts (Fig. 11*A*, cut *C*; six tested cells), response amplitudes to stimulation sites 19–26 were not different from those observed in control slices at the same recording site and stimulation intensity (5.4 ± 1.12 vs 5.77 ± 0.84 mV in control and experimental slices, respectively; Student's unpaired t test, $p > 0.05$). In contrast, all neurons recorded after cut *B* ($n = 7$) were unresponsive to these stimuli (Fig. 11*B*) even with stimulation intensities as high as 1.2 mA. Response amplitudes to stimulation sites 1–18 were similar to those obtained in control slices.

Further attempts to identify the trajectory of the longitudinal axons conveying distant neocortical inputs gave ambiguous results. Indeed, after cuts D or E, half of the cells (four tested cells in each condition) remained responsive to sites 19–26, suggesting that axons coursing in the perirhinal cortex and the external capsule convey long-range neocortical influences.

DISCUSSION

This study was undertaken to examine the rostrocaudal propagation and postsynaptic effects of neocortical inputs to the perirhinal cortex. Our findings can be summarized as follows. First, activation of a point source in the neocortex elicits synaptic responses in RS neurons located throughout the perirhinal cortex via longitudinal axonal pathways coursing in the perirhinal cortex itself and/or in the external capsule. Second, the responses of RS

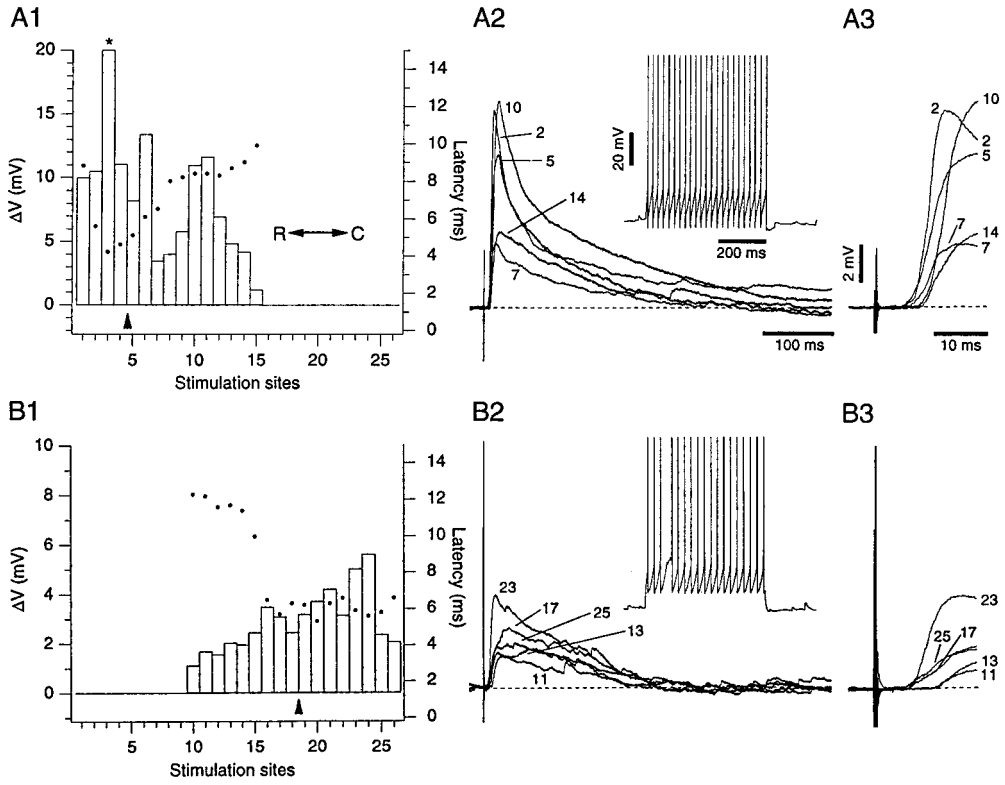

Figure 9. Synaptic responses of FS perirhinal neurons to electrical stimuli applied in the neocortex. *A* and *B* represent two different neurons. *1A1*, *B1*, Graphs plotting the peak amplitude (*bars*, *left axis*) of evoked synaptic potentials as a function of the stimulation site (average of four responses). The onset latency of the EPSPs is also indicated (*dots*, *right axis*). Note the lack of evoked IPSPs from this V_m (−65 mV). The position of the recorded cells with respect to the stimulation sites is indicated by a *triangle* at the *bottom* of each graph. *A2–3*, *B2–3*, Synaptic responses elicited by selected stimulation sites (*numbers*) depicted with a slow (*2*) and fast (*3*) time base (single sweeps). The *insets* in *2* illustrate the first response to depolarizing current injections eliciting more than one spike from rest. Calibration bars in *A* are also valid for *B*. The *asterisk* in *A1* marks a suprathreshold response. In *A–B*, rest was −68 and −64 mV, respectively.

cells depend on whether they are in transverse register with the activated neocortical site or not: responses to adjacent sites are composed of excitatory and inhibitory components, whereas responses to distant ones (≥1 mm) lack an inhibitory component. Third, in keeping with the above, the rostrocaudal extent of stimulating sites eliciting EPSPs is more restricted in presumed inhibitory interneurons than in principal cells. This suggests that the longitudinal pathways conveying long-range neocortical influences do not contact inhibitory interneurons.

In the following account, we will consider these findings in light of relevant anatomical and physiological data and discuss their relevance for associative processes.

Propagation of neocortical inputs along the longitudinal axis of the perirhinal cortex

That neocortical inputs could propagate extensively in the rostrocaudal axis is surprising given the limited thickness of perirhinal slices. However, several factors suggest that this result is not caused by the spurious activation of perirhinal cells by current spread from the stimulating electrodes. First, stimulation intensities as low as 1.2 times those required to elicit a response at the neocortical site closest to the recorded cell were sufficient to elicit a fully propagating response. Second, if the propagation was caused by the diffuse activation of perirhinal neurons at different levels of the perirhinal slice, similar responses should have been evoked from most sites. Instead, the character of the response depended on the position of the stimulation site: adjacent sites elicited a mixed excitatory–inhibitory response, whereas distant ones evoked only depolarizing potentials. Moreover, response latencies increased with the distance between the stimulating and recording sites. Third, interrupting longitudinal axons coursing in the perirhinal cortex itself and in the external capsule blocked the propagation, whereas neocortical cuts had no effect, also inconsistent with the idea that current spread was involved. Finally, glutamate microinjections at different rostrocaudal levels of the neocortex could reproduce the results obtained with electrical stimuli.

In fact, our results are supported by physiological and anatomical data. Indeed, a recent current source density analysis in the whole guinea pig brain kept *in vitro* has revealed that superficial neocortical stimuli evoke responses that spread longitudinally in the perirhinal cortex (Biella et al., 2000). Moreover, tract tracing studies indicate that many perirhinal cells have longitudinal axons spanning large extents of the perirhinal cortex (Witter et al., 1986). However, although neocortical inputs tend to focus on particular perirhinal levels, evidence of rostrocaudal divergence was also obtained (Deacon et al., 1983; Room and Groenewegen, 1986; Burwell and Amaral, 1998b). Although the methods used in the present study preclude determination of the fiber system(s) allowing the rostrocaudal propagation, we feel that longitudinal perirhinal axons represent the most likely candidate, in keeping with the results of our lesion experiments.

The responses of perirhinal cells to neocortical stimuli depend on their position relative to neocortical stimulation sites

As mentioned above, neocortical stimulation sites elicited mixed excitatory–inhibitory responses or only depolarizing potentials, depending on whether they were in rostrocaudal register with the recorded cell or not, respectively. It appears unlikely that this is a consequence of differences in the intensity of the synaptic volley, because reducing the stimulation intensity at adjacent sites or increasing that at distant sites failed to change the character of the responses. Another explanation, namely that adjacent electrical stimuli had a higher probability of backfiring perirhinal cells with excitatory axonal collaterals to inhibitory interneurons, seems unlikely because local glutamate application in the neocortex could reproduce the effects of electrical stimuli. By exclusion,

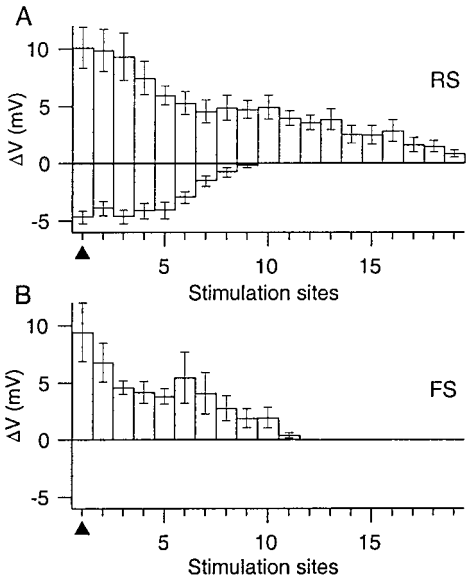

Figure 10. Average response profile of RS (*A*) and FS (*B*) neurons to neocortical stimuli. Subsets of RS ($n = 8$) and FS ($n = 5$) neurons were recorded 1.12 mm (or 7 stimulation sites) or less from either extremity of the stimulating electrode array. Response profiles were averaged after aligning the data with respect to the position of the cells (*filled triangles* at the level of stimulation site 1).

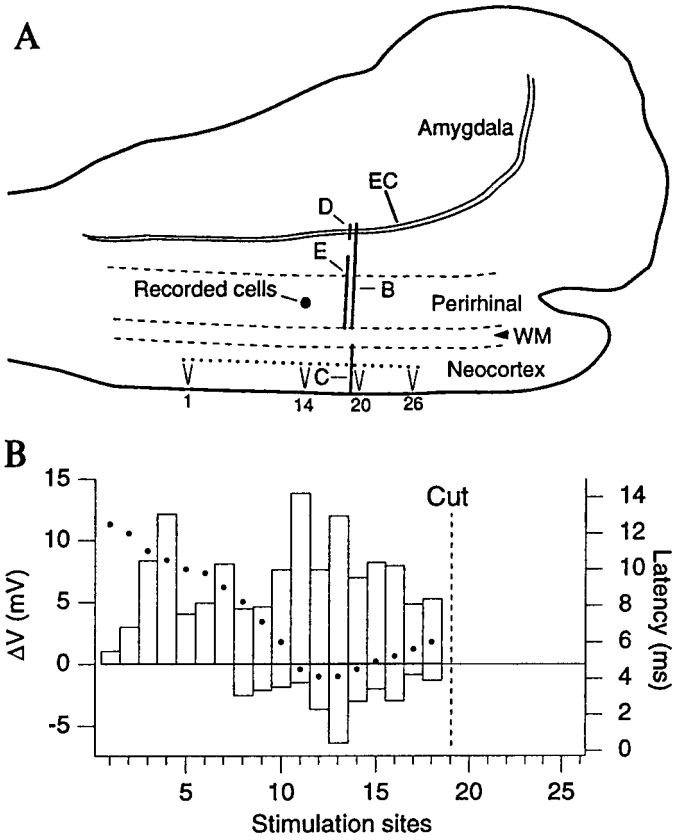

Figure 11. The rostrocaudal propagation of neocortical inputs in the perirhinal cortex does not depend on axons coursing longitudinally in the neocortex. The scheme in *A* shows the experimental paradigm used in this series of experiments. RS perirhinal neurons were recorded at the level of stimulating site 14, the midpoint of the electrode array. Before positioning the stimulation electrodes, at the level of site 20, small cuts were performed in the perirhinal cortex and external capsule (cut *B*), in the neocortex (cut *C*), and in external capsule or the perirhinal cortex, separately (cuts *D* and *E*, respectively). The *graph* in *B* plots the peak amplitude of evoked synaptic potentials (*bars*, *left axis*) as a function of the stimulation site in an RS neuron recorded after a cut *B*. The onset latency of the EPSPs is also indicated (*dots*, *right axis*). Note abolition of responses rostral to the cut. In contrast, cut *C* (in the neocortex) did not abolish the responses.

we are left with the intriguing possibility that pathways conveying long- and short-range neocortical influences, respectively, form and do not form synaptic contacts with inhibitory neurons, as indicated by the more restricted rostrocaudal extent of neocortical stimuli affecting FS cells.

A critical question here is whether the exact angle of the slice might account for this phenomenon. Indeed, it is conceivable that small deviations of the slices' angle with respect to the lamination of the perirhinal cortex could account for the more restricted response profile of FS cells. However, this explanation would necessitate that the longitudinal axons spread very little in the different cortical laminae, a condition inconsistent with the available anatomical data (Witter et al., 1986). Also, it is possible that the longer intrinsic axon collaterals were damaged during slicing, leading to a progressive reduction in the probability of interneuron innervation with distance. However, the fact that distal stimuli could evoke large EPSPs in RS cells argues against this possibility.

Thus, our physiological data support the notion that long-range horizontal perirhinal axons do not contact inhibitory interneurons, whereas short-range perirhinal axons and neocortical axons do. This interpretation is supported by our study of anterogradely labeled longitudinal axons of the perirhinal area (Martina et al., 2000). In this study, we found that the vast majority of elements postsynaptic to intrinsic terminals were dendritic spines, whereas inhibitory local-circuit cells are generally aspiny (Ribak, 1978; Freund et al., 1983).

In this context, it should be pointed out that similar conclusions were reached for amygdala projections to the perirhinal cortex and insula (Smith and Paré, 1994; Paré et al., 1995). Moreover, there are precedents in the literature of intrinsic cortical projections targeting mostly spines. In the prefrontal cortex, for instance, Melchitzky et al. (1998) reported that dendritic spines constitute the prevalent target of intrinsic pyramidal axons (96% of postsynaptic elements), a conclusion supported by a subsequent electrophysiological study (González-Burgos et al., 2000). However, other data suggest that this phenomenon might be limited to high-order cortical areas. In the primary visual (Kisvárday et al., 1986; Gabbott et al., 1987; McGuire et al., 1991), somatosensory (Elhanany and White, 1990; White and Czeiger, 1991), and motor cortices (Keller and Asanuma, 1993), a lower proportion of elements postsynaptic to intrinsic axons contributed by pyramidal neurons are dendritic spines (~75–90%), with no difference between proximal and distal projections.

Implications for associative memory

Our results suggest that neocortical inputs reaching different transverse levels of the perirhinal cortex can be distributed longitudinally via an intrinsic system of perirhinal connections. As a result, transversely distributed activation patterns representing sensory information about the same or different modalities can converge on subsets of perirhinal cells. Moreover, the fact that short- and long-range pathways conveying neocortical inputs are differentially related to inhibitory interneurons implies that the perirhinal circuitry is biased to favor associative interactions.

Indeed, activation of a point source in the neocortex will recruit perirhinal inhibitory interneurons at the corresponding transverse level, thus limiting the depolarization of principal cells by cortical afferents. In contrast, simultaneous activation of two distant neocortical sites will shift the balance toward excitation in perirhinal cells receiving direct neocortical inputs because long-range intrinsic pathways do not engage inhibitory interneurons.

The significance of these findings derives from the hypothesized role of coincident neuronal activity in NMDA-dependent synaptic plasticity (Bliss and Collingridge, 1993; Malenka and Nicoll, 1993) and evidence indicating that this mechanism is at play in the perirhinal cortex (Bilkey, 1996; Ziakopoulos et al., 1999). The excitatory action of intrinsic perirhinal axons might be required to bring about the activity-dependent changes in synaptic weights that have been hypothesized to underlie associative memory (Hebb, 1949). Moreover, because the intrinsic pathways linking different transverse perirhinal levels are reciprocal, subsequent activation of one site might be sufficient to reactivate the entire distributed pattern.

Given the strong reciprocal connections existing between the perirhinal cortex, on the one hand, and the entorhino-hippocampal system and amygdala (see references in introductory remarks), on the other, it appears likely that these structures cooperate in various forms of learning (Eichenbaum, 1997; Cahill, 2000). This is consistent with recent findings indicating that the perirhinal cortex (Collins et al., 1999), lateral nucleus of the amygdala (Paré and Collins, 2000), and entorhino-hippocampal system (Green and Arduini, 1954; Mitchell and Ranck, 1980; Buzsáki et al., 1983; Alonso and García-Austt, 1987) oscillate at the theta frequency during attentive states. In this context, an attractive possibility would be that coherent theta oscillations reinforce in the time domain what these structures allow in space with their profuse intrinsic connectivity.

REFERENCES

Alonso A, García-Austt E (1987) Neuronal sources of theta rhythm in the entorhinal cortex of the rat. Exp Brain Res 67:493–501.

Beggs JM, Kairiss EW (1994) Electrophysiology and morphology of neurons in rat perirhinal cortex. Brain Res 665:18–32.

Biella G, Uva L, deCurtis M (2000) Associative potentials in the pathway from the neocortex to the entorhinal cortex of the guinea pig. Soc Neurosci Abstr 26:703.

Bilkey DK (1996) Long-term potentiation in the in vitro perirhinal cortex displays associative properties. Brain Res 733:297–300.

Bliss T, Collingridge GL (1993) A synaptic model of memory: long-term potentiation in the hippocampus. Nature 361:31–39.

Buckley MJ, Gaffan D (1998) Learning and transfer of object-reward associations and the role of the perirhinal cortex. Behav Neurosci 112:15–23.

Bunsey M, Eichenbaum H (1993) Critical role of the parahippocampal region for paired-associate learning in rats. Behav Neurosci 107:740–747.

Burwell RD, Amaral DG (1998a) Perirhinal and postrhinal cortices of the rat: interconnectivity and connections with the entorhinal cortex. J Comp Neurol 391:293–321.

Burwell RD, Amaral DG (1998b) Cortical afferents of the perirhinal, postrhinal, and entorhinal cortices of the rat. J Comp Neurol 398:179–205.

Buzsáki G, Leung L, Vanderwolf CH (1983) Cellular bases of hippocampal EEG in the behaving rat. Brain Res Rev 6:139–171.

Cahill L (2000) Modulation of long-term memory storage in humans by emotional arousal: adrenergic activation and the amygdala. In: The amygdala: a functional analysis (Aggleton JP, ed), pp 425–445. Oxford: Oxford UP.

Collins DR, Lang EJ, Paré D (1999) Spontaneous activity of the perirhinal cortex in behaving cats. Neuroscience 89:1025–1039.

Connors BW, Gutnick MJ, Prince DA (1982) Electrophysiological properties of neocortical neurons in vitro. J Neurophysiol 48:1302–1320.

Deacon TW, Eichenbaum H, Rosenberg P, Eckman KW (1983) Afferent connections of the perirhinal cortex in the rat. J Comp Neurol 220:168–190.

Dutar P, Nicoll RA (1988) A physiological role for GABA B receptors in the central nervous system. Nature 332:156–158.

Eacott MJ, Gaffan D, Murray EA (1994) Preserved recognition memory for small sets, and impaired stimulus identification for large sets, following rhinal cortex ablations in monkeys. Eur J Neurosci 6:1466–1478.

Eichenbaum H (1993) Thinking about brain cell assemblies. Science 261:993–994.

Eichenbaum H (1997) How does the brain organize memories? Science 277:330–332.

Elhanany E, White EL (1990) Intrinsic circuitry: synapses involving the local axon collaterals of corticocortical projection neurons in the mouse primary somatosensory cortex. J Comp Neurol 291:43–54.

Faulkner B, Brown TH (1999) Morphology and physiology of neurons in the rat perirhinal-lateral amygdala area. J Comp Neurol 411:613–642.

Freund TF, Martin KAC, Smith AD, Somogyi P (1983) Glutamate decarboxylase-immunoreactive terminals of Golgi-impregnated axoaxonic cells and of presumed basket cells in synaptic contact with pyramidal neurons of the cat's visual cortex. J Comp Neurol 221:263–278.

Gabbott PLA, Martin KAC, Whitteridge D (1987) Connections between pyramidal neurons in layer V of cat visual cortex (area 17). J Comp Neurol 259:364–381.

González-Burgos G, Barrionuevo G, Lewis DA (2000) Horizontal synaptic connections in monkey prefrontal cortex: an in vitro electrophysiological study. Cereb Cortex 10:82–92.

Green JD, Arduini AA (1954) Hippocampal electrical activity in arousal. J Neurophysiol 17:533–557.

Hebb DO (1949) The organization of behavior. New York: Wiley.

Herzog C, Otto T (1997) Odor-guided fear conditioning in rats: 2. Lesions of the anterior perirhinal cortex disrupt fear conditioned to the explicit conditioned stimulus but not to the training context. Behav Neurosci 111:1265–1272.

Higuchi S, Miyashita Y (1996) Formation of mnemonic neuronal responses to visual paired associates in inferotemporal cortex is impaired by perirhinal and entorhinal lesions. Proc Natl Acad Sci USA 93:739–743.

Insausti R, Amaral DG, Cowan WM (1987) The entorhinal cortex of the monkey. II. Cortical afferents. J Comp Neurol 264:356–395.

Jones EG, Powell TPS (1970) An anatomical study of converging sensory pathways within the cerebral cortex of the monkey. Brain 93:793–820.

Keller A, Asanuma H (1993) Synaptic relationships involving local axon collaterals of pyramidal neurons in the cat motor cortex. J Comp Neurol 336:229–242.

Kisvárday ZF, Martin KAC, Freund TF, Maglóczky Z, Whitteridge D, Somogyi P (1986) Synaptic targets of HRP-filled layer III pyramidal cells in the cat striate cortex. Exp Brain Res 64:541–552.

Malenka RC, Nicoll RA (1993) NMDA-receptor-dependent synaptic plasticity: multiple forms and mechanisms. Trends Neurosci 16:521–527.

Martina M, Royer S, Paré JF, Smith Y, Paré D (2000) Perirhinal propagation of neocortical inputs. Soc Neurosci Abstr 26:470.

McCormick DA (1989) GABA as an inhibitory transmitter in human cerebral cortex. J Neurophysiol 62:1018–1027.

McCormick DA, Connors BW, Lightall JW, Prince DA (1985) Comparative electrophysiology of pyramidal and sparsely spiny stellate neurons of the neocortex. J Neurophysiol 54:782–806.

McGuire BA, Gilbert CD, Rivlin PK, Wiesel TN (1991) Targets of horizontal connections in macaque monkey primary visual cortex. J Comp Neurol 305:370–392.

Melchitzky DS, Sesack SR, Pucak ML, Lewis DA (1998) Synaptic targets of pyramidal neurons providing intrinsic horizontal connections in monkey prefrontal cortex. J Comp Neurol 390:211–224.

Meunier M, Bachevalier J, Mishkin M, Murray EA (1993) Effects on visual recognition of combined and separate ablations of the entorhinal and perirhinal cortex in rhesus monkeys. J Neurosci 13:5418–5432.

Meunier M, Hadfield W, Bachevalier J, Murray EA (1996) Effects of rhinal cortex lesions combined with hippocampectomy on visual recognition memory in rhesus monkeys. J Neurophysiol 75:1190–1205.

Mitchell S, Ranck JB (1980) Generation of theta rhythm in medial entorhinal cortex of freely moving rats. Brain Res 189:49–66.

Mumby DG, Pinel J (1994) Rhinal cortex lesions and object recognition in rats. Behav Neurosci 108:11–18.

Nuñez A, Amzica F, Steriade M (1993) Electrophysiology of cat association cortical cells in vivo: intrinsic properties and synaptic responses. J Neurophysiol 70:418–429.

Paré D, Collins DR (2000) Neuronal correlates of fear in the lateral amygdala: multiple extracellular recordings in conscious cats. J Neurosci 20:2701–2710.

Paré D, Smith Y, Paré JF (1995) Intra-amygdaloid projections of the basolateral and basomedial nuclei in the cat: *Phaseolus vulgaris*-leucoagglutinin anterograde tracing at the light and electron microscopic level. Neuroscience 69:567–583.

Ribak CE (1978) Aspinous and sparsely-spinous stellate neurons in the

visual cortex of rats contain glutamic acid decarboxylase. J Neurocytol 7:461–478.
Room P, Groenewegen HJ (1986) Connections of the parahippocampal cortex. I. Cortical afferents. J Comp Neurol 251:415–450.
Scanziani M, Gähwiler BH, Thompson SM (1991) Paroxysmal inhibitory potentials mediated by $GABA_B$ receptors in partially disinhibited rat hippocampal slice cultures. J Physiol (Lond) 444:375–396.
Schwindt P, O'Brien JA, Crill W (1997) Quantitative analysis of firing properties of pyramidal neurons from layer 5 of rat sensorimotor cortex. J Neurophysiol 77:2484–2498.
Shi CJ, Cassell MD (1999) Perirhinal cortex projections to the amygdaloid complex and hippocampal formation in the rat. J Comp Neurol 406:299–328.
Smith Y, Paré D (1994) Intra-amygdaloid projections of the lateral nucleus in the cat: PHA-L anterograde labeling combined with postembedding GABA and glutamate immunocytochemistry. J Comp Neurol 342:232–248.
Stafstrom CE, Schwindt PC, Flatman JA, Crill WE (1984) Properties of subthreshold response and action potential recorded in layer V neurons from cat sensorimotor cortex in vitro. J Neurophysiol 52:244–263.
Suzuki WA (1996) The anatomy, physiology and functions of the perirhinal cortex. Curr Opin Neurobiol 6:179–186.
Suzuki WA, Amaral DG (1994a) Perirhinal and parahippocampal cortices of the macaque monkey: cortical afferents. J Comp Neurol 350:497–533.
Suzuki WA, Amaral DG (1994b) Topographic organization of the reciprocal connections between the monkey entorhinal cortex and the perirhinal and parahippocampal cortices. J Neurosci 14:1854–1877.
Suzuki WA, Zola-Morgan S, Squire LR, Amaral DG (1993) Lesions of the perirhinal and parahippocampal cortices in the monkey produce long-lasting memory impairment in the visual and tactual modalities. J Neurosci 13:2430–2451.
Van Hoesen GW, Pandya DN (1975) Some connections of the entorhinal (area 28) and perirhinal (area 35) cortices of the rhesus monkey. I. Temporal lobe afferents. Brain Res 95:1–24.
White EL, Czeiger D (1991) Synapses made by axons of callosal projection neurons in mouse somatosensory cortex: emphasis on intrinsic connections. J Comp Neurol 303:233–244.
Witter MP, Groenewegen HJ (1986) Connections of the parahippocampal cortex in the cat. III. Cortical and thalamic efferents. J Comp Neurol 252:1–31.
Witter MP, Room P, Groenewegen HJ, Lohman AHM (1986) Connections of the parahippocampal cortex in the cat. V. Intrinsic connections; comments on input/output connections with the hippocampus. J Comp Neurol 252:78–94.
Ziakopoulos Z, Tillett CW, Brown MW, Bashir ZI (1999) Input- and layer-dependent synaptic plasticity in the rat perirhinal cortex in vitro. Neuroscience 92:459–472.
Zola-Morgan S, Squire LR (1993) Neuroanatomy of memory. Annu Rev Neurosci 16:547–563.
Zola-Morgan S, Squire LR, Amaral DG, Suzuki WA (1989) Lesions of perirhinal and parahippocampal cortex that spare the amygdala and hippocampal formation produce severe memory impairment. J Neurosci 9:4355–4370.
Zola-Morgan S, Squire LR, Clower RP, Rempel NL (1993) Damage to the perirhinal cortex exacerbates memory impairment following lesions to the hippocampal formation. J Neurosci 13:251–265.